Nanoscale

Accepted Manuscript

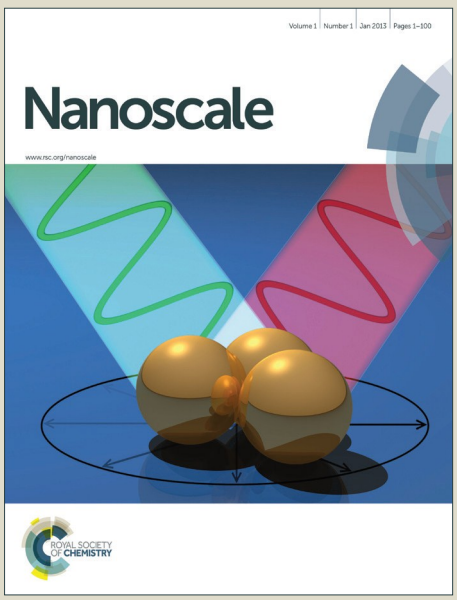

ROYAL SOCIETY OF CHEMISTRY

www.rsc.org/nanoscale

Journal Name

ARTICLE

Highly narrow nanogap-containing Au@Au core-shell SERS nanoparticles: Size-dependent Raman enhancement and applications in cancer cell imaging

Received 00th January 20xx,
Accepted 00th January 20xx

DOI: 10.1039/x0xx00000x

www.rsc.org/

Chongya Hu, ‡[a] Jianlei Shen, ‡[c] Juan Yan,*[b] Jian Zhong,[b] Weiwei Qin,[c] Rui Liu,[b] Ali Aldalbahi,[d] Xiaolei Zuo,[c] Shiping Song,[c] Chunhai Fan[c] and Dannong He*[ab]

Cellular imaging technologies employing metallic Surface-enhanced Raman scattering (SERS) tags have gained much interest toward clinical diagnositics, but they are still suffering from poor controlled distribution of hot spots and reproducibility of SERS signals. Here, we report the fabrication and characterization of high narrow nanogap-containing Au@Au core-shell SERS nanoparticles (GCNPs) for the identification and imaging of protein overexpressed on the surface of cancer cells. First, plasmonic nanostructures are made of gold nanoparticles (~ 1 nm) coated with gold shells, between which a highly narrow and uniform nanogap (~1.1 nm) is formed owing to polyA anchored on the Au cores. Well controlled distribution of Raman reporter molecules, such as 4, 4'-dipyridyl (44DP) and 5, 5'-dithiobis (2-nitrobenzoic acid) (DTNB) which are readily encoded in the nanogap and can generate strong, reproducible SERS signals. In addition, we have investigated the size-dependent SERS activity of GCNPs and found that with a same laser wavelength, the Raman enhancement discriminated particle sizes. The maximum Raman enhancement was achieved at a certain threshold of particle size (~76 nm). High narrow nanogap-containing Au@Au core-shell SERS tags (GCTs) were prepared via the functionalization of hyaluronic acid (HA) on GCNPs, which recognized CD44 receptor, a tumor-associated surface biomarker. And it was showed GCTs had a good targeting ability to tumour cells and promising prospect for multiplex biomarkers detection.

Introduction

Cellular imaging aims to develop new methods and technologies for the accurate identification and discrimination of normal from tumour cells or pathological tissues, and to develop effective solutions to improve cancer diagnosis accuracy and subsequent disease management.[1-4] Among the methods and technologies,[5-9] Surface-enhanced Raman scattering (SERS),[10-15] an ultrasensitive vibrational spectroscopic technique, has attracted considerable attention due to its many outstanding advantages over existing imaging techniques.[16-18] Most SERS substrates have an improved detection sensitivity that can reach 4-6 orders of magnitude higher than conventional Raman spectroscopy, and there're even reports of up to 14 orders of magnitude,[19] which is comparable with or even better than fluorescence detection. Moreover, the extremely short lifetimes of SERS prevent photobleaching in the excited state and render higher photostability than fluorescence methods.[20] Metal nanosubstrate, such as gold (Au) and silver (Ag) nanoparticle (NP), which act as structural scaffolds for Raman signal amplification is one essential part in a SERS system.

However, the simple metal NP-Raman reporter structure cannot generate a reproducible and uniform response owing to randomly distributed hot sports which are regarded to induce enormous electromagnetic enhancement.[16, 21-24] In addition, there is a common drawback that in all cases the metal surface is unprotected, allowing the possibility for components of the analyte to adsorb on the metal surface, potentially replacing the label species and generally decreasing the reliability of the assay.[25] Also, it usually lacks stability, and the signal is easily disturbed by surrounding interference.[26] Hence, coating materials are designed, and a typical "SERS tag" can be developed after a biorecognition element is employed subsequently.[27] Despite ultrasensitive, multiplex and biocompatible properties of SERS tags,[28-31] researches in this area has fallen behind that of other nanoprobes such as quantum dots (QDs) and dye-doped nanobeads.[32] One reason for this is complex and delicate steps and still unsolved problem of uncontrollable distribution of hot spots.[16, 27] The other is that Raman dyes in the inner metal materials render the chemical

[a] School of Materials Science and Engineering, Shanghai Jiao Tong University, Shanghai 200240, China. E-mail: hdn_nercn@163.com
[b] National Engineering Research Center for Nanotechnology, Shanghai 200241, China. E-mail: yjsinap@163.com
[c] Division of Physical Biology & Bioimaging Center, Shanghai Synchrotron Radiation Facility, Shanghai Institute of Applied Physics, Chinese Academy of Sciences, Shanghai 201800, China
[d] Chemistry Department, King Saud University, P.O. Box 2455, Riyadh 11451, Saudi Arabia
†Electronic Supplementary Information (ESI) available: See DOI: 10.1039/x0xx00000x
‡ These authors contributed equally to this work.

enhancement inoperable as a SERS mechanism.[33] Recently well-defined gold nanobridged nanogap particles were reported[34] to show strong, highly quantitative and controllable SERS signals.[35] However, several critical techniques still remain challenging, including forming GCTs in different particle sizes easily and controllably, functionalizing the GCNPs to prepare GCTs to produce strong and stable SERS signals for cellular imaging.

Herein, we report a controllable and convenient synthetic route of GCNPs, which can mediate interior nanogap through a short period of polyA and incorporate the Raman reporter molecules in the nanogaps. The obtained single gold (core)-gold (shell) nanogap-containing particles can be functionalized further with hyaluronic acid (HA) and used as SERS tags. Human colon carcinoma cells (HCT 116 cells) with overexpressed CD44 (an HA receptor) were used as the model target cells, and the targeting ability of the proposed GCTs was examined. The concept behind this approach is illustrated in Fig.1

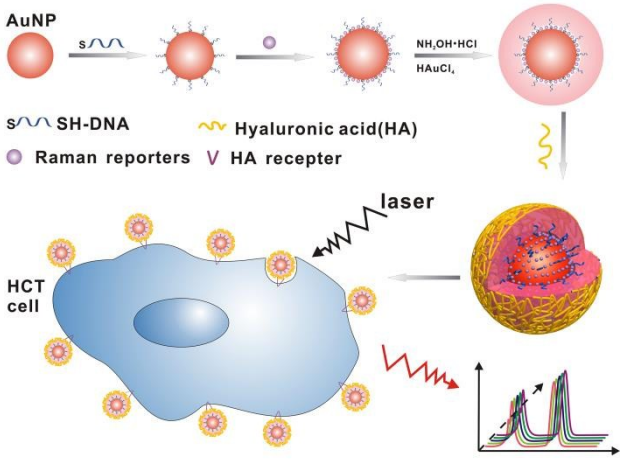

Fig.1 Schematic illustration of the synthetic procedures of GCNPs and GCTs for specific recognition of cancer cells. HCT cells: Human colon carcinoma cells.

Results and Discussion

Fig. 1 depicts the assembly process of GCNPs. In this method, thiol-30 adenines (SH-polyA$_{30}$) were anchored on the surface of AuNPs (~15nm) via the bond between Au-S. Then, two kinds of non-fluorescent small Raman reporter molecules, 4, 4'-dipyridyl (44DP), and 5, 5'-dithiobis (2-nitrobenzoic acid) (DTNB) were chosen and adsorbed onto the remaining surface of the AuNP-DNA nanocomposites. Afterwards, we used SH-polyA- and Raman molecules-modified AuNPs as seeds to synthesize a gold shell, with subsequent addition of polymer (polyvinylpyrrolidone, PVP), reductant (hydroxylamine hydrochloride, NH_2OH-HCl) and gold precursor (chloroauric acid solution, $HAuCl_4$). Synthetic details can be found in the Supplementary Information. The structures of the GCNPs were confirmed by UV-vis spectroscopy, Nano-ZS ZEN3600 particle sizer, Scanning electron microscopy (SEM) and high-resolution transmission electron microscopy (HRTEM).

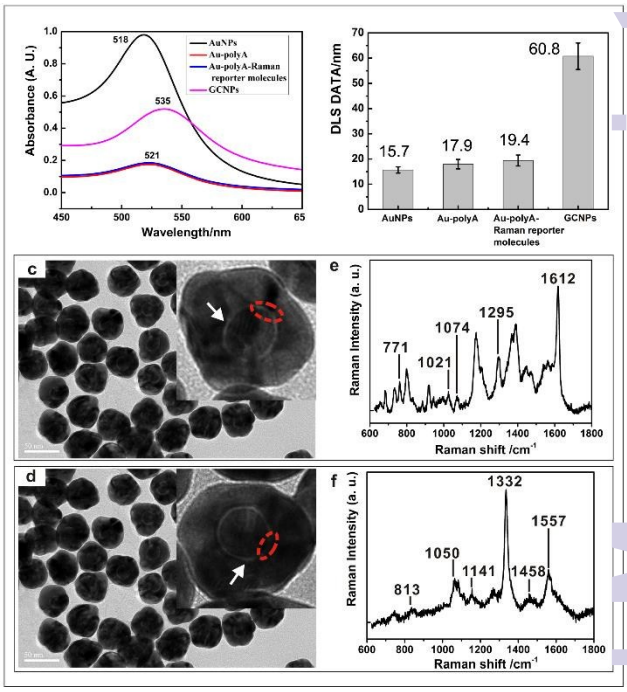

Fig. 2 Characterization of nanoparticles. a, UV-vis spectra for the NPs. b Hydrodynamic radii of four nanostructures (Au, Au-polyA, Au-polyA-rama reporters, and GCNPs) determined using dynamic light scattering (DLS). Error ba represent the standard deviation of three independent measurements. c-d, HRTEM image of the GCNPs encoded with 44DP and DTNB as raman report molecules separately. The inset shows the nanogaps and bridges (white arr and red dotted circles) in more detail. e-f, The corresponding SERS spectra of particles in c and d respectively. All spectra were acquired with a 633 nm excitatio laser, at 300 mW, and for a 10 s exposure for a single spectrum for 100 s, with t same particle concentration (1 nM).

The AuNPs first show the absorbance with a peak at 518 nm and then the absorbance red shift from 518 to 535 nm as the formation of nanoshell (Fig. 2a). It was reported tha intermediates were formed during the synthetic process whose plasmatic resonance at ~680 nm disappeared when the fin products were formed completely,[35] which means the characteristic gold shell plasmatic properties began to gov the overall spectra. The UV-vis spectrum of core-shell structures with a broader peak shape than that of AuNPs in our research is consistent with that published previously.[35]

In addition, dynamic light scattering (DLS) experiments were then conducted to confirm the growth of Au nanocores a measure changes in the hydrodynamic radii of the followin different nanoparticles: AuNPs, AuNPs-polyA, AuNPs-polyA Raman molecules, and GCNPs (Fig. 2b). The hydrodynamic rad of those NPs which change from about 15.7 nm to 60.8 nm correlated well with the UV-vis spectra. Moreover, SEM image in Fig. S1† shows two different GCNPs encoded with 44DP an DTNB separately displayed good dispersion with a uniform diameter.

Importantly, those particles have a uniform interior nanoga as shown in the HRTEM images in Fig. 2c-d (white arrows), an the average gap size were determined to be ~1.18 nm and ~1.09 nm (Fig. S2†). Furthermore, a bridge was found between th core and shell (red dotted circles) where the gold was first

loaded onto the AuNPs and then grew on its surface. Several works reported fabricating nanomaterials with structural order, such as Au@Ag core-shell structures, mediated by the different surface ligands.[36, 37] It was concluded that polyA used in the synthetic process was a key surface material in forming the nanogap-containing particles. First, thiol groups have a strong binding affinity to gold via chemisorptions with strength approaching that of a covalent bond. Furthermore, the relative adsorption affinity of oligo (dA) on Au surface was reported to strongly dominate over the other oligonucleotides.[38] Hence, polyAs were prone to be a layer on the surface of Au which might block the direct deposition of gold onto the gold seed surface. Gold precursors must attach to the initial nucleation sites which generated a bridge, grow over the polyA layer and lead to the formation of interior nanogaps finally.[39] Fig. 2e and Fig. 2f show the normal Raman spectra of molecular 44DP and DTNB encoded in the GCNPs. The feature peaks were 771, 1021, 1074, 1295, 1612cm^{-1} for 44DP and 813, 1050, 1141, 1332, 1458, 1557cm^{-1} for DTNB, which were consistent with those previously reported.[39, 40] The calculated near-field electromagnetic field of the GCNPs by the finite-difference time-domain (FDTD) method also confirmed the formation of nanogaps (Fig. S3†) and the EF (enhancement factor) value of the GCNPs was calculated as 0.93×10^6. (The calculation can be found in the Supporting Information)

It was ever reported that "hot spots" in nanogaps area contribute a lot to SERS intensity.[41] Actually, it also has been demonstrated that particle sizes of colloidal metal nanoparticles is a key structural parameter in determining SERS enhancements.[42] Herein, we used GCNPs to illustrate whether or not there are the size dependent SERS activities likewise for interior gap-containing metal nanoparticles. In practice, when citrate-stabilized ~15 nm AuNPs were used as seeds (Fig. 3a), depending on the amount of $HAuCl_4$ added, uniform gold nanoshell were formed on the gold core surface with tuneable thickness. We deliberately synthesized GCNPs with 13 kinds of different sizes (Mean particle diameters): 40.7 nm, 45.1 nm, 50.3 nm, 53.25 nm, 56.18 nm, 62.17 nm, 69.14 nm, 76.79 nm, 76.87 nm, 81.23 nm, 85.76 nm, 89.21 nm, and 99.64nm respectively which were imaged using TEM (Fig. 3b-n). The colour of the nanoparticles solution changed from pink (~15 nm) to dark red (~99 nm), color deepening gradually with the increase of the nanoparticles sizes (Fig. 3o). Fig. 3p showed the changes of Raman spectra with the increase of the NPs size with the excitation of 633 nm laser. It can be observed when the size reaching ~76 nm, the SERS activity reached a maximum at the characteristic peak 1332 cm^{-1} for 44DP. It is worth mentioning that there was no obvious SERS signal of DNA bases (polyA) had been detected. (Fig. S4†) After this threshold size, it decreased (Fig. 3q)The mechanism of size-dependent Raman enhancement for Au@Ag core-shell nanoparticles was ever explained by Cheng's group in 2015.[43] Plasmon hybridizat model which demonstrates the interaction between th plasmons of metallic nanostructures is regarded to contribut to the Raman enhancement. With the increase of metallic she thickness, the intensity of antibonding plasmons will exhib appreciable increase due to the fact that the internal and external energy modes are closer. However, when it reaches t a threshold, resonance of metallic shell grows as strong as that of pure metal nanoparticles with the energy dissipation in th core. Hence, the plasmatic resonance, as well as the SERS activity decreases. In fact, we found a similar trend in SERS intensity for GCNPs when nanoshell thickness changes. The SERS activity increased when NPs sizes increased, and when reached a threshold size (~76 nm), the SERS activity decreased It can be concluded that when the metallic shell thickness wa ~61 nm, the internal and external energy modes are closes which resulted to the best SERS activity for GCNPs.

The as-prepared GCNPs (~76 nm) were functionalized with HA, forming GCTs for targeting and recognizing tumour cell practical use. Actually, before that, we first examined the cytotoxicity of the prepared structures in HCT116 cells. found that the bare GCTs did not cause evident inhibition of th proliferation of HCT116 cells (Fig. S5†), indicating their excellent biocompatibility which is consistent with many related report about pure AuNPs.[44] HA is known to be a major constituent vertebrate tissue and body fluid, and also play an important role in various biological processes. Beyond this, HA is also known t be an attractive targeting ligand that binds CD44 receptors, which are overexpressed in many kinds of tumour cell Therefore, HA has been widely utilized as a cancer targeting moiety for imaging, drug delivery applications.[45]

According to the results in Fig. 6S†, the UV-vis spectra and hydrodynamic radii results shows the change in the size afte the modification with HA. Furthermore, as shown in Fig. 7S†, compared with the original HA and β-mercaptoethylamine, th prepared nanogap-containing SERS tags showed new peaks at ~1615 cm^{-1} , ~2863 cm^{-1}, and ~2916 cm^{-1} attributed to the characteristic absorption peaks of HA and β mercaptoethylamine in the FT-IR spectra. These result confirmed that GCNPs were conjugated to HA successfully.

To verify the targeting ability of HA, Laser Scanning Confoca Microscope (LSCM) images were taken of HCT 1116 cell sample after treatment with GCTs for 0.5h. HA molecules and GCNP were employed as controls. When the excitation was set a 633nm, the blue fluorescence was from 4, 6-diamino-2-phenyl indole (DAPI) and the red was from SERS tags in the

Journal Name

ARTICLE

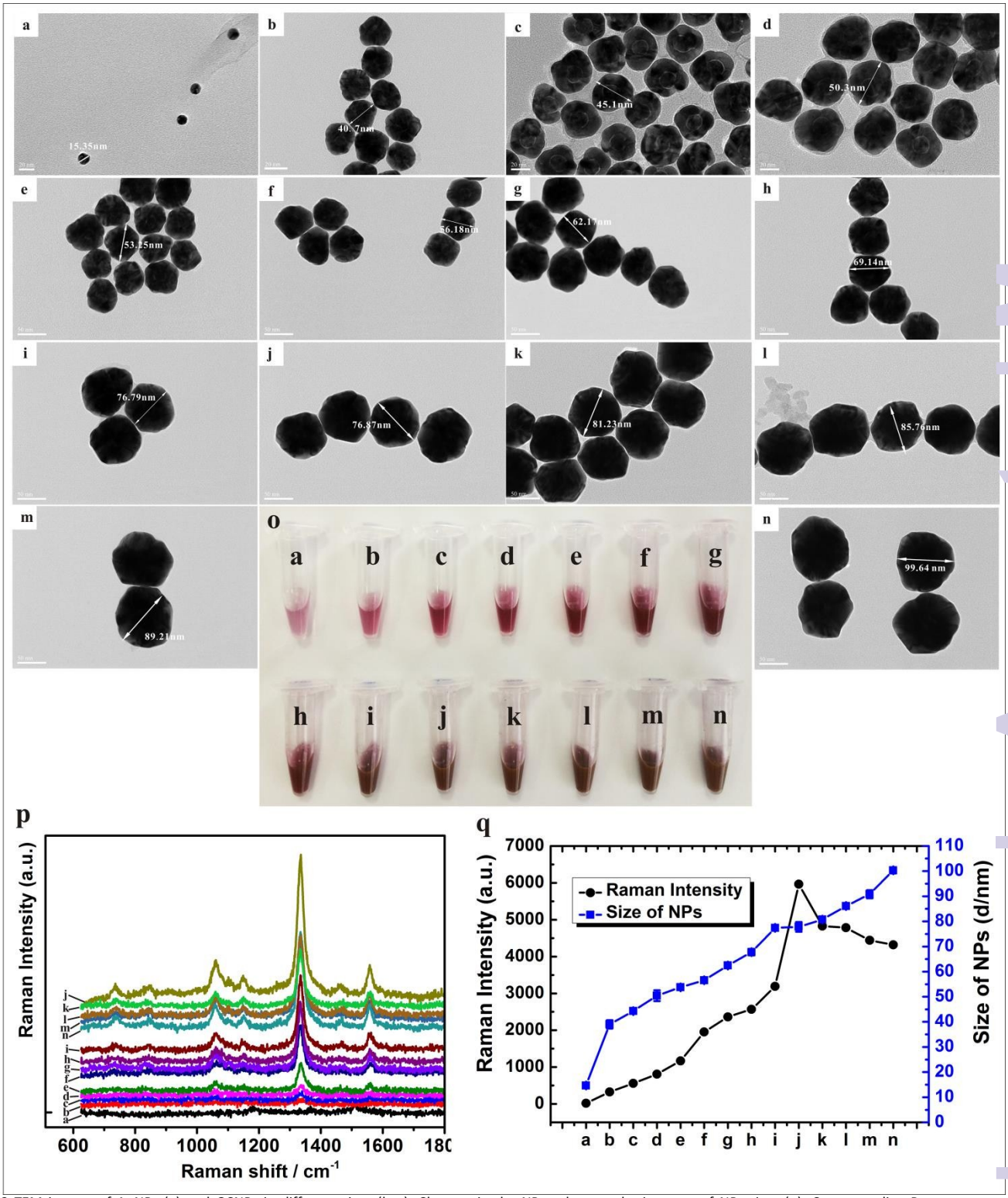

Fig. 3 TEM images of AuNPs (a) and GCNPs in different sizes (b-n); Changes in the NPs colour as the increase of NPs sizes (o); Corresponding Raman spectra of experimental NPs (p); SERS intensity at peak 1332 cm^{-1} based on increasing sizes of NPs under the laser of 633 nm. Error bars represent the standard deviation of t...

independent measurements.

reflection mode of LSCM. The discrete red dots indicated that the GCTs remained on the surface of HCT 116 cells, which meant that GCTs could target and recognize the receptor of CD44 on the surface of tumour cells successfully, showing a high targeting specificity. As shown in Fig. 4, HA and GCNPs-treated cells exhibited no fluorescence. Furthermore, dark-field images of GCTs-treated cell lines clearly show obvious light scattering from the HCT 116 cells (Fig. 5c) comparing with healthy cells HEK293 (Fig. 5a). In addition, GCNPs-treated HCT116 cells exhibited no discernible light scattering either (Fig. 5b). This result clearly shows the good specificity and efficient targeting ability of GCTs conjugating to tumour cells.

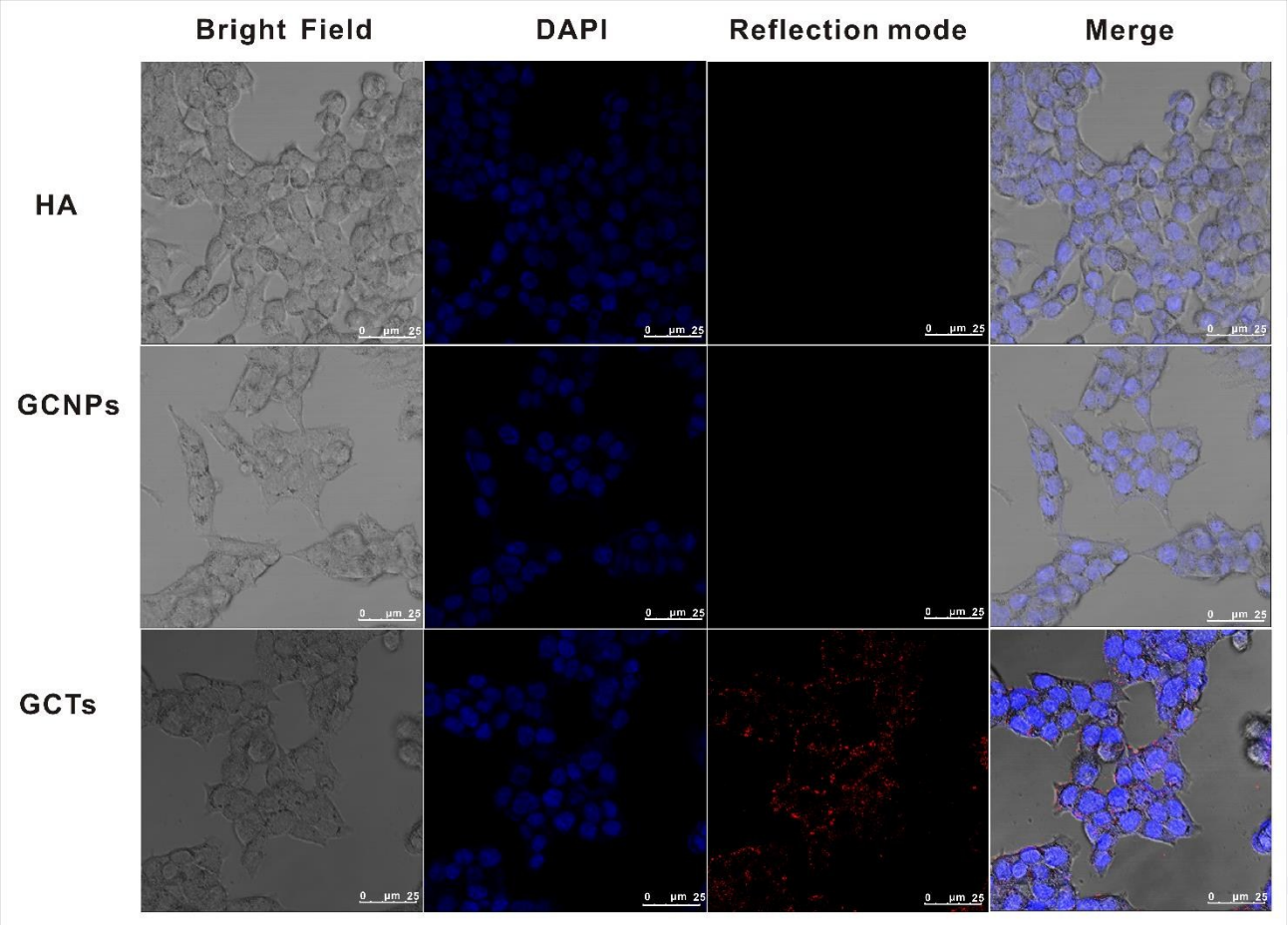

Fig. 4 Confocal imaging of living HCT116 cells treated with HA, GCNPs, and GCTs. The final concentration of HA and nanoparticles were 0.2 nM and 1 nM respectively. The emission wavelength was 633 nm, and the detection wavelength was 613~653 nm.

Actually, a variety of fluorescent dyes, such as conventional fluorescent dyes and quantum dots (QDs) have been applied widely for cellular imaging. However, their applications still suffer from various problems, including photobleaching, poor photostability and cytotoxicity.[46, 47] Moreover, when irradiated under the laser, many fluorescent dye molecules would further generate cytotoxin-like singlet oxygen and free radicals.[48] The performance of GCTs for the detection of biomarkers (CD44) on the surface of the HCT116 cells was then investigated by a streamline Raman mapping system. To validate the multiplex detection capability of prepared SERS tags, 44DP and DTNB were co-encoded on the surface of Au cores simultaneously. The detection results are shown in Fig. 6. Fig. 6a shows the optical image of a single HCT116 cell and the Raman spectra from two different areas (indicated with yellow circles and numbered with 1 and 2) are shown in Fig.6b. It could be seen that the spectra have a very good signal-to-noise ratio, suggesting that the enhancement from GCTs were uniform and strong. Fig. 6c and Fig. 6d represent the Raman mapping images of CD44 on the single HCT116 cell, which were prepared by integrating the area under the characteristic peaks (1612 cm-1 for 44DP and 1332 cm-1 for DTNB). However, GCNPs-treated HCT116 cells and GCTs- treated healthy cells exhibited no discernible signals either (Fig. S8†). According to

Journal Name

ARTICLE

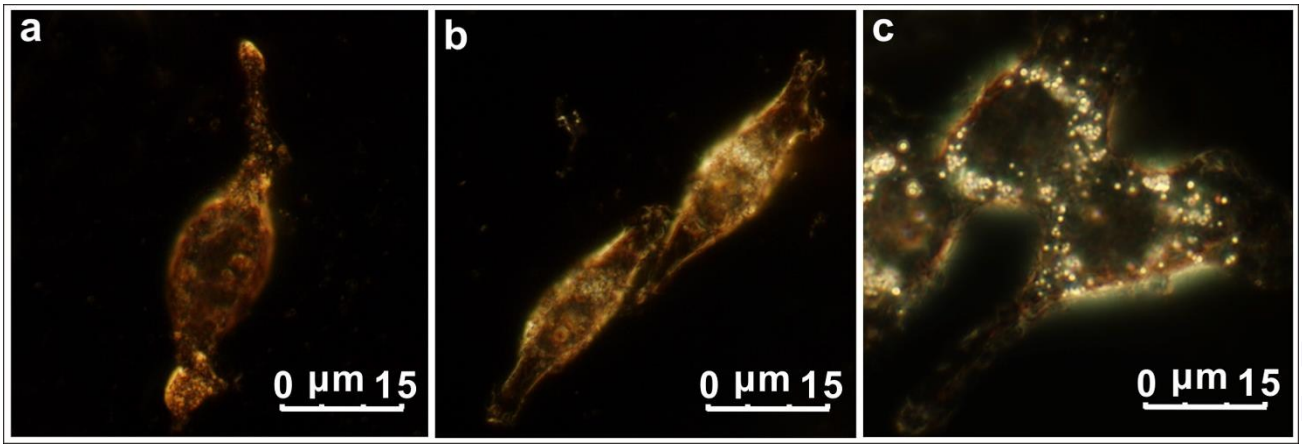

Fig. 5 Dark field image of healthy cells treated with GCTs (a) for 0.5h; Dark-field images of HCT116 cells after incubating GCNPs (b) and GCTs for o.5h (c).

the results, it can be concluded that it not only illustrated the distribution of CD44 but also showed the potential ability of duplex imaging of dual markers overexpressed on the surface of tumour cells, which makes this an ideal platform for detection of multiplex biomarkers.

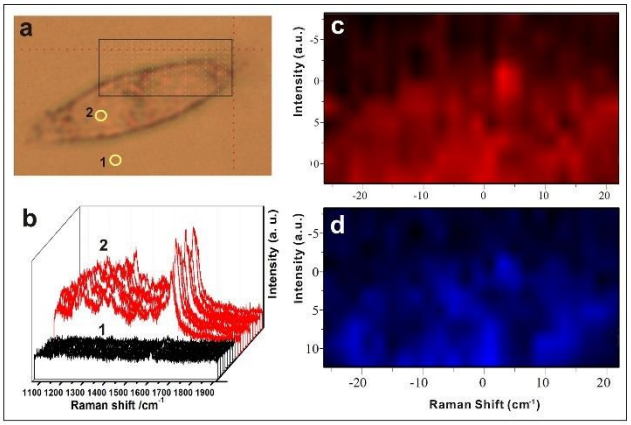

Fig. 6 a, Opitcal image of a single HCT116 cell; b, Corresponding SERS spectra of HCT116 cells at two different areas indicated with yellow circles, illustrating the signal reproducibility. c-d, Raman mapping images of GCTs distributed on single HCT116 cell surface under the characteristic peaks (1612 cm^{-1} for 44DP and 1332 cm^{-1} for DTNB);

Conclusions

In summary, we have demonstrated an efficient strategy for the size-dependent SERS activities of plasmonic GCNPs towards detection of tumour cells. Monodisperse GCNPs were synthesized with well controlled sizes by coating gold shells in different thickness. GCNPs with diameter of about 76 nm, which achieved the maximized Raman enhancement, were used as SERS tags for targeting and imaging specific cancer markers in living cells after modified with HA. According to our results, it is clearly showed that GCTs have advantages over other reporte probes. First, Firm Au-S bond and strong affinity of polyA on Au surface make Au seeds superior dispersibility and stability whi is important for the following growth of metallic shells. Secon high controllability of hot spots owing to the interior nanoga leads to highly uniform and reproducible SERS signals. Third excellent biocompatibility and photostability compared t fluorescent probes. Moreover, they can be readil functionalized with selected binding ligands to perm simultaneous multiplexed determination of two or mor biomarkers on the cell surface. According to our results in th experiment, not only a new method for uniform nanogaps but also novel GCNPs were proposed which would be used as ideal candidate for simultaneous bioimaging and SERS detection for the early diagnosi of cancers.

Acknowledgements

We would like to thank the National Basic Research Program o China (973 program, no. 2013CB932500) and the National Science Foundation of China (21305088, 51073173), Shangh Science and Technology Development Funds (13QB1402100) for financial support.

Notes and references

1. S. Casciaro, *World J Radiol*, 2011, **3**, 249-255.
2. R. Jandial, *Neurosurgery*, 2009, **64**, N13-14.
3. P. Lang, K. Yeow, A. Nichols and A. Scheer, *Nat. Rev. Dru Discov.*, 2006, **5**, 343-356.
4. P. Mitchell, *Nat. Biotechnol.*, 2001, **19**, 1013-1017.

5. A. Ostrowski, D. Nordmeyer, A. Boreham, C. Holzhausen, L. Mundhenk, C. Graf, M. C. Meinke, A. Vogt, S. Hadam, J. Lademann, E. Ruhl, U. Alexiev and A. D. Gruber, *Beilstein J Nanotechnol*, 2015, **6**, 263-280.
6. H. Xu, Q. Li, L. Wang, Y. He, J. Shi, B. Tang and C. Fan, *Chem. Soc. Rev.*, 2014, **43**, 2650-2661.
7. D. K. Welsh and T. Noguchi, *Cold Spring Harb. Protoc.*, 2012, **2012**.
8. K. Kikuchi, *Adv. Biochem. Eng. Biotechnol.*, 2010, **119**, 63-78.
9. S. B. Rizvi, S. Ghaderi, M. Keshtgar and A. M. Seifalian, *Nano Rev*, 2010, **1**.
10. K. Kneipp, Y. Wang, H. Kneipp, L. T. Perelman, I. Itzkan, R. R. Dasari and M. S. Feld, *Phys. Rev. Lett.*, 1997, **78**, 1667-1670.
11. J. Kneipp, H. Kneipp and K. Kneipp, *Chem. Soc. Rev.*, 2008, **37**, 1052-1060.
12. P. L. Stiles, J. A. Dieringer, N. C. Shah and R. P. Van Duyne, *Annu. Rev. Anal. Chem.*, 2008, **1**, 601-626.
13. S. Schlücker, *Angewandte Chemie International Edition*, 2014, **53**, 4756-4795.
14. J. Ando and K. Fujita, *Curr. Pharm. Biotechnol.*, 2013, **14**, 141-149.
15. M. M. Harper, K. S. McKeating and K. Faulds, *Phys. Chem. Chem. Phys.*, 2013, **15**, 5312-5328.
16. D. Radziuk and H. Moehwald, *Phys. Chem. Chem. Phys.*, 2015.
17. A. F. Palonpon, J. Ando, H. Yamakoshi, K. Dodo, M. Sodeoka, S. Kawata and K. Fujita, *Nat. Protoc.*, 2013, **8**, 677-692.
18. D. C. Kennedy, K. A. Hoop, L. L. Tay and J. P. Pezacki, *Nanoscale*, 2010, **2**, 1413-1416.
19. A. M. Michaels, Jiang and L. Brus, *The Journal of Physical Chemistry B*, 2000, **104**, 11965-11971.
20. W. E. Doering and S. Nie, *Anal. Chem.*, 2003, **75**, 6171-6176.
21. K. A. Willets, *Chem. Soc. Rev.*, 2014, **43**, 3854-3864.
22. S. M. Stranahan and K. A. Willets, *Nano Lett.*, 2010, **10**, 3777-3784.
23. J. P. Camden, J. A. Dieringer, Y. Wang, D. J. Masiello, L. D. Marks, G. C. Schatz and R. P. Van Duyne, *J. Am. Chem. Soc.*, 2008, **130**, 12616-12617.
24. S. J. Lee, A. R. Morrill and M. Moskovits, *J. Am. Chem. Soc.*, 2006, **128**, 2200-2201.
25. A. Shen, L. Chen, W. Xie, J. Hu, A. Zeng, R. Richards and J. Hu, *Adv. Funct. Mater.*, 2010, **20**, 969-975.
26. Y. Wang, B. Yan and L. Chen, *Chem. Rev.*, 2013, **113**, 1391-1428.
27. J. Ni, R. J. Lipert, G. B. Dawson and M. D. Porter, *Anal. Chem.*, 1999, **71**, 4903-4908.
28. C. L. Zavaleta, B. R. Smith, I. Walton, W. Doering, G. Davis, B. Shojaei, M. J. Natan and S. S. Gambhir, *Proc. Natl. Acad. Sci. U. S. A.*, 2009, **106**, 13511-13516.
29. S. Lee, H. Chon, S. Y. Yoon, E. K. Lee, S. I. Chang, D. W. Lim and J. Choo, *Nanoscale*, 2012, **4**, 124-129.
30. A. Samanta, K. K. Maiti, K. S. Soh, X. Liao, M. Vendrell, U. S. Dinish, S. W. Yun, R. Bhuvaneswari, H. Kim, S. Rautela, J. Chung, M. Olivo and Y. T. Chang, *Angew. Chem. Int. Ed. Engl.*, 2011, **50**, 6089-6092.
31. X. Qian, X. H. Peng, D. O. Ansari, Q. Yin-Goen, G. Z. Chen, D. M. Shin, L. Yang, A. N. Young, M. D. Wang and S. Nie, *Nat. Biotechnol.*, 2008, **26**, 83-90.
32. D. O. Ansari, *Ph.D. dissertation, Georgia Institute of Technology, Atlanta*, **September 16, 2008**.
33. L. Guerrini and D. Graham, *Chem. Soc. Rev.*, 2012, **41**, 703[illegible] 7107.
34. Z. Zhang, S. Zhang and M. Lin, *Chem. Commun.*, 2013, **49**, 8519-8521.
35. D. K. Lim, K. S. Jeon, J. H. Hwang, H. Kim, S. Kwon, Y. D. Suh and J. M. Nam, *Nat. Nanotechnol.*, 2011, **6**, 452-460.
36. Y. Feng, J. He, H. Wang, Y. Y. Tay, H. Sun, L. Zhu and H. Chen, *J. Am. Chem. Soc.*, 2012, **134**, 2004-2007.
37. L. H. Tan, H. Xing, H. Chen and Y. Lu, *J. Am. Chem. Soc.*, 2013, **135**, 17675-17678.
38. H. Kimura-Suda, D. Y. Petrovykh, M. J. Tarlov and L. J. Whitman, *J. Am. Chem. Soc.*, 2003, **125**, 9014-9015.
39. B. Zhao, J. Shen, S. Chen, D. Wang, F. Li, S. Mathur, S. Song and C. Fan, *Chemical Science*, 2014, **5**, 4460-4466.
40. C. C. Lin and C. W. Chang, *Biosens. Bioelectron.*, 2014, **51**, 297-303.
41. J. Shen, J. Su, J. Yan, B. Zhao, D. Wang, S. Wang, K. Li, M. [illegible] Y. He, S. Mathur, C. Fan and S. Song, *nano research*, 2015, **8**, 731-742.
42. C. E. Talley, J. B. Jackson, C. Oubre, N. K. Grady, C. W. Hollars, S. M. Lane, T. R. Huser, P. Nordlander and N. J. Halas, *Nano Lett.*, 2005, **5**, 1569-1574.
43. P. Guo, D. Sikdar, X. Huang, K. J. Si, W. Xiong, S. Gong, L. W. Yap, M. Premaratne and W. Cheng, *Nanoscale*, 2015, **7**, 2862-2868.
44. Y. Zhao, X. Gu, H. Ma, X. He, M. Liu and Y. Ding, *The Journal of Physical Chemistry C*, 2011, **115**, 12797-12802.
45. J. Li, Y. He, W. Sun, Y. Luo, H. Cai, Y. Pan, M. Shen, J. Xia and X. Shi, *Biomaterials*, 2014, **35**, 3666-3677.
46. J. Yan, M. Hu, D. Li, Y. He, R. Zhao, X. Jiang, S. Song, L. Wang and C. Fan, *nano research*, 2008, **1**, 490-496.
47. Y. Su, M. Hu, C. Fan, Y. He, Q. Li, W. Li, L. H. Wang, P. Shen and Q. Huang, *Biomaterials*, 2010, **31**, 4829-4834.
48. X. Ragas, A. Jimenez-Banzo, D. Sanchez-Garcia, X. Batllori and S. Nonell, *Chem. Commun.*, 2009, 2920-2922.